Topological nature of the class of antiperovskite alkaline earth-pnictide compounds

Wen Fong Goh and Warren E. Pickett
Department of Physics, University of California, Davis CA 95616, USA
(Dated: December 2, 2016)

The antiperovskite structure class $Ae_3Pn_APn_B$ of alkaline earth (Ae = Ca,Sr,Ba) pnictides (Pn = N,P,As,Sb,Bi) compounds has been shown by Sun and collaborators[1] to harbor topological insulating phases. We provide a density functional based survey of this entire class of $3 \times 5 \times 5$ compounds, determining first the relative energetic stability of the distribution of pairs of Pn ions in the A and B sites of the structure, then analyse the electronic structure and topological characteristics of those stable structures. Taking advantage of inversion symmetry, the Z_2 topological invariants are obtained from the parity of the occupied bands at the time-reversal invariant momenta (TRIMs). The effects of spin-orbit coupling and strain on the topological nature are described. A case study of Ca_3BiP including the effect of strain illustrates how a topological semimetal can be transformed into topological insulator, producing the topologically protected surface state, and also into Dirac semimetal, where the Dirac points are protected by the crystal symmtery.

PACS numbers:

I. INTRODUCTION

Topological insulators (TIs) have an entanglement of valence and conduction bands that must become disentangled at an interface to vacuum (*i.e.* at a surface), giving rise to topologically protected gapless, conducting surface states. There are three primary classes of TIs. A two dimensional Chern insulator, which has magnetism (broken time reversal symmetry) and an associated integer Chern number, displays a quantized quantum anomalous Hall conductance. In three dimensions (3D), a Z_2 topological insulator (TI) is characterized by a Z_2 index, while a topological crystalline insulator (TCI)[3] is characterized by a mirror Chern number. Both have gapless edge states, protected by either time-reversal symmetry (former) or mirror symmetry (latter), providing a quantum spin Hall (QSH) character. In 3D, a Z_2 strong and weak topological insulator is distinguished from a normal insulator by four independent Z_2 invariants $\nu_0; \nu_1\nu_2\nu_3$. If $\nu_0 = 1$, it is a strong topological insulator (STI); if $\nu_0 = 0$, it could be a weak topological insulator if one of the rest of the ν are non-zero, otherwise it is a trivial insulator.

To date many structural classes of topological insulators have been discovered, including HgTe[4], $Bi_{1-x}Sb_x$ alloy[5], Bi_2Se_3 and Sb_2Te_3 family,[6–8], Sr_3Bi_2[9], and others.[10] Some, for example, HgTe and $\alpha - Sn$ (gray tin) require strain to induce a topologically non-trivial energy gap, while others, like Bi_2Te_3, Bi_2Se_3 and Sb_2Te_3 are STIs with rhombohedral structure, yet all follow the band inversion mechanism. Experimental methods like angle resolved photoemission spectroscopy (ARPES) and scanning tunneling microscopy (STM) are used to identify the topological surface states. Currently, there are more than thirty TI materials[10] that have been addressed experimentally, including $Bi_{1-x}Sb_x$ alloy[5], the first 3D topological insulator to be verified experimentally.

In spite of these many classes of TIs, the search for new classes of TIs continues. One important factor is that most existing TIs are defective and not insulating enough in the bulk to allow study of their surface bands, or to consider the applications that seemed to be promised for TIs. One recipe for finding new TIs is to look for insulators that have valence bands and conduction bands with opposite parity and with small or negative gaps. For very small gap materials, the bands may be inverted by spin orbit-coupling (SOC) leading to insulating gaps that may house topological states. In this case the band gap (without SOC) must be small enough for band inversion, while large enough to have application at room temperature. The other possibility is to have a band overlap semimetal (before SOC), with a gap opened at the Fermi level by SOC. In both cases the strength of SOC governs the magnitude of gap that can be obtained. This realization has focused attention on heavy atoms with large SOC.

Here we consider in some generality pnictides with the antiperovskite structure, for which some examples have been suggested to be potential topological insulators. Certain oxides, for example the alkaline earth based Sr_3PbO, have been calculated to be TCIs,[11] while the monovalent based nitride Cu_3PdN is calculated to be a topological node-line semimetal.[12] Bismuth and nitride based antiperovskite compounds[1] as well as cesium and iodine based perovskite compounds[13] have been proposed to be STIs under the application of strain. Yet many antiperovskite materials are found to be just topologically trivial.

Motivated by these findings, we have carried out a survey on the entire class of $3 \times 5 \times 5$ alkaline earth-pnictide antiperovskite compounds, viz. $Ae_3Pn_APn_B$, where Ae = Ca, Sr, Ba and Pn_A, Pn_B = N, P, As, Sb, Bi, using first principles density functional theory (DFT) methods. The conventional ordering of elements Ae, Pn_A, and Pn_B follows that of a perovskite with general chemical formula of ABO_3, where the A cation is 12-fold cuboctahedral coordinated and B is 6-fold coordinated, surrounded by an octahedron of O anions. In the case of antiperovskite $Ae_3Pn_APn_B$, Pn_B is inside the Ae_6 oc-

tahedron while Pn_A sits in the more open A site. Our study shows that these cubic antiperovskite compounds can be either trivial insulators or topological semimetals, and can be classified into three categories. The term topological semimetal refers to three classes of topological materials. First, a semimetal consists of electron and hole pockets, or in other words, a negative band gap, with non-zero topological invariant. Second, a semiconductor with zero band gap that possesses non-trivial topological phase. The gap could be opened by lowering the crystal symmetry. Third, a Dirac/Weyl/Nodal-line semimetal, where chiral edge states emerge by breaking either time-reversal symmetry or inversion symmetry. Throughout this paper, we use the term topological semimetal to refer to the first and second types. By applying uniaxial strain along certain directions, some topological semimetals transit into a topological insulating phase.

II. THEORY AND METHODOLOGY

A. Band inversion mechanism

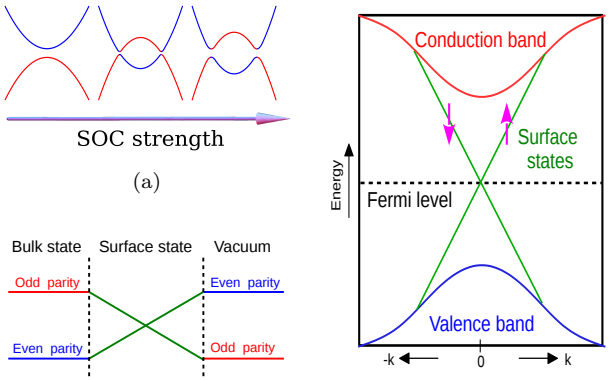

FIG. 1: Schematic diagrams show the relation between topological surface states and band inversion. (a) Bands with opposite parity (indicated by blue and red) are inverted by spin-orbit coupling. (b) Surface states formed by 'connecting' the bands with similar parity. (c) Ideal topological surface states protected by the time-reversal symmetry.

The band topology of TIs is characterized by band inversion. A schematic diagram in Fig. 1a explains the band inversion mechanism behind the topological insulator. For an insulator with a small band gap, as the SOC strength increases, the band gap closes and the bands touch each other until they eventually overlap. Since SOC also lowers the symmetry, the degeneracy at the band crossings will be lifted. If an insulator has opposite parity for valence and conduction bands, the bands could be inverted and this results in a topologically non-trivial phase.

When these inverted bands are projected onto a surface contacting with a (trivial) insulator or vacuum, topological surface bands could be formed on the surface with band dispersion crossing the bulk band gap (Fig. 1b). These topological surface states (Fig. 1c) are protected by the time-reversal symmetry:

$$\varepsilon(k,\uparrow) = \varepsilon(-k,\downarrow) \tag{1}$$

The analysis of the band topology can be made by calculating the Z_2 topological invariants. For systems with inversion symmetry, Fu and Kane[14] showed that the topological invariants can be deduced from the parity eigenvalues of the occupied bands at time-reversal invariant momenta (TRIMs). There are eight TRIMs in a 3D cubic system at Γ : (000), X : (100), (010), (001), M : (110), (101), (011) and A : (111).

B. Methods

To study the electronic structure of the *Ae-Pn* antiperovskites, a first principles DFT method is used within the generalized gradient approximation (GGA) exchange correlation of Perdew-Burke-Ernzerhof-1996[16] implemented in the Full-Potential Local-Orbital Minimum-Basis (FPLO)[17] scheme on a k-mesh of $20\times20\times20$. The full relativistic band calculations for SOC implemented in FPLO are performed by solving the four-component Kohn-Sham-Dirac equation.

III. ANALYSIS OF RESULTS

A. Cell volume and energetic stability

A cubic antiperovskite $Ae_3Pn_APn_B$ structure[15] (space group $Pm\bar{3}m$) has an Ae_6Pn_B octahedron, with Pn_A surrounded symmetrically by eight octahedra, as in Fig. 2a. Thus positions of cations and anions are interchanged compared to the large class of perovskite oxides. For the cubic (undistorted) structure, the equilibrium lattice constant has been obtained for all $3\times5\times5$ combinations. These results and the following data are presented in Table I. First is a comparison of the energy difference upon interchange of the two Pn ions. It is always the case that it is energetically favorable to have the smaller Pn ion in the Pn_B octahedron position. Energy differences, which range from 0.2-4.3 eV, are largest when N is one of the ions, and the magnitude of the difference increases with difference in atomic number of the anions. These trends can be understood from classical Coulomb energies from formal valences. If the smaller anion is surrounded by the cation octahedron, the distance of separation between the anion and cation is smaller, leading to larger Coulombic attraction and a more stable state.

TABLE I: Data on the complete class of $Ae_3Pn_APn_B$ antiperovskites. a(Å) gives the optimized lattice constants in Å. $\Delta E = E_{Ae_3Pn_APn_B} - E_{Ae_3Pn_BPn_A}$ provides the energy difference in eV. Since this energy difference is antisymmetric across the diagonal, the energy differences are only shown in the lower left triangle for the stable phase (the smaller Pn ion is always Pn_B). ε_g and ε_g^{SOC} give the band gap (without and with SOC) in eV; of either a small positive or negative (negative indirect band gap) value, with an exception of a few with bands crossing at the Fermi level or gapless states (represented by SM for semimetallic or M for metallic state). Only the ν_0 Z_2 index is provided, because all $\nu_{1,2,3}$ are zero. Values in bold indicate a topological semimetal state.

		N_B					P_B					As_B					Sb_B					Bi_B				
		a(Å)	ΔE(eV)	ε_g(eV)	ε_g^{SOC}(eV)	Z_2	a(Å)	ΔE(eV)	ε_g(eV)	ε_g^{SOC}(eV)	Z_2	a(Å)	ΔE(eV)	ε_g(eV)	ε_g^{SOC}(eV)	Z_2	a(Å)	ΔE(eV)	ε_g(eV)	ε_g^{SOC}(eV)	Z_2	a(Å)	ΔE(eV)	ε_g(eV)	ε_g^{SOC}(eV)	Z_2
N_A	Ca	4.61	-	0.	0.	1	5.29	-	SM	M	1	5.42	-	0.	0.	1	5.76	-	-0.01	-0.02	1	5.85	-	-0.01	-0.04	1
	Sr	4.99	-	0.	0.	1	5.67	-	0.	0.	1	5.80	-	0.	-0.01	1	6.13	-	-0.02	-0.03	1	6.23	-	-0.02	-0.05	1
	Ba	5.33	-	SM	SM	1	6.03	-	-0.04	-0.05	1	6.18	-	-0.05	-0.06	1	6.52	-	-0.07	-0.08	1	6.61	-	-0.05	-0.12	1
P_A	Ca	4.73	-2.96	0.85	0.85	0	5.31	-	0.33	0.31	0	5.42	-	0.10	0.05	0	5.74	-	0.	0.	1	5.82	-	0.	0.	1
	Sr	5.09	-2.55	0.45	0.45	0	5.67	-	0.	0.	1	5.79	-	0.	0.	1	6.09	-	0.	0.	1	6.17	-	0.	0.	1
	Ba	5.43	-2.28	SM	SM	0	6.02	-	0.03	0.01	1	6.14	-	0.	0.	1	6.44	-	0.	0.	1	6.53	-	0.	-0.10	1
As_A	Ca	4.78	-3.38	0.77	0.72	0	5.34	-0.55	0.15	0.09	0	5.45	-	0.	0.	1	5.75	-	0.	0.	1	5.84	-	0.	0.	1
	Sr	5.13	-2.93	0.30	0.28	0	5.70	-0.50	0.	0.	**1**	5.81	-	0.	0.	1	6.11	-	0.	0.	1	6.19	-	0.	-0.01	1
	Ba	5.47	-2.64	SM	SM	0	6.04	-0.46	0.	0.	**1**	6.16	-	0.	0.	1	6.46	-	0.	-0.02	1	6.54	-	0.	-0.14	1
Sb_A	Ca	4.88	-4.26	0.46	0.35	0	5.39	-1.76	0.65	0.50	0	5.49	-1.2	0.40	0.22	0	5.78	-	0.07	0.	1	5.86	-	0.	0.	1
	Sr	5.22	-3.77	0.20	0.15	0	5.74	-1.58	0.30	0.16	0	5.84	-1.08	0.10	0.	**1**	6.13	-	0.	0.	1	6.21	-	0.	0.	1
	Ba	5.55	-3.40	SM	SM	0	6.08	-1.45	0.28	0.18	0	6.19	-0.99	0.13	0	**1**	6.48	-	0.	0.	1	6.55	-	0.	-0.12	1
Bi_A	Ca	4.92	-4.35	0.48	0.07	0	5.42	-1.99	0.16	0.	**1**	5.53	-1.44	0.	-0.03	**1**	5.81	-0.29	0.	-0.10	**1**	5.89	-	0.	-0.12	0
	Sr	5.26	-3.86	0.25	0.01	0	5.77	-1.75	0.	-0.02	**1**	5.88	-1.26	0.	-0.05	**1**	6.15	-0.20	0.	-0.10	**1**	6.23	-	0.	-0.13	0
	Ba	5.59	-3.47	SM	SM	0	6.11	-1.61	0.	-0.05	**1**	6.22	-1.17	0.	-0.10	**1**	6.50	-0.21	0.	-0.18	**1**	6.58	-	0.	-0.17	0

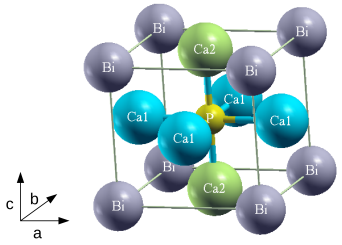

(a) Tetragonal crystal structure of strained Ca_3BiP.

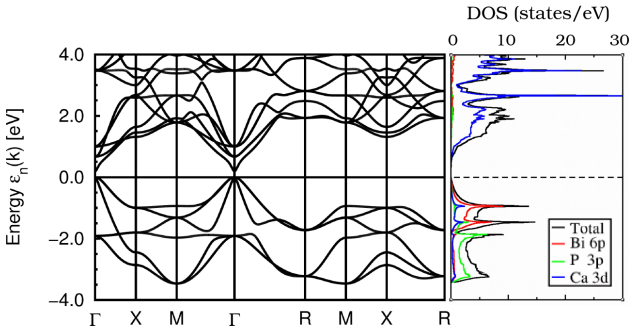

(b) Band structure and density of states of cubic Ca_3BiP.

FIG. 2: (a) Antiperovskite structure of Ca_3BiP with tetragonal compression of 5% along (001), space group becomes $P4/mmm$. Ca atoms become two nonequivalent atoms (blue and green). (b) Band structure and density of states of cubic Ca_3BiP (without SOC). P 3p bands occupy the lowest valence states, while Bi 6p bands occupy the highest valence states. Ca 4s and 3d bands occupy the conduction states and seperate the valence states by 0.2 eV.

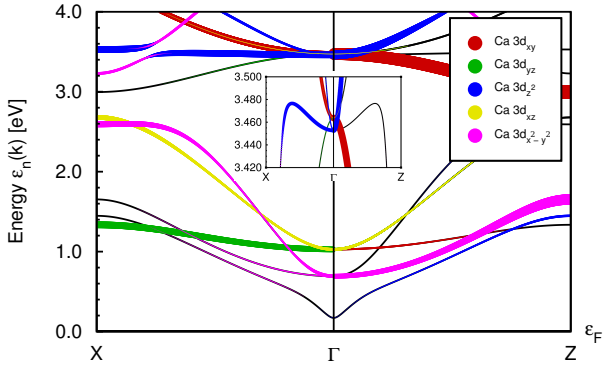

FIG. 3: The ordering of Ca $(\frac{1}{2}, \frac{1}{2}, 0)$ d-orbital energies at Γ point is consistent with the tight binding model. Insert: d_{xy} and d_{z^2} are not generate at Γ point. Notation: X=(100), Γ=(000) and Z=(001).

B. Electronic band structure

The electronic structure and DOS of a representative compound, Ca_3BiP, shown in Fig. 2b, reveal that the smaller Pn_B p bands lie lower than the Pn_A p bands, making the latter ion the one of interest in determining the band gap (or not) and subsequently the topological character. Both p bands have 3-fold degeneracy at Γ point. In the conduction bands Ae d bands appear, along with some "free electron like" bands that have no majority orbital character. To understand the ordering of the cation d-characters at Γ point, the fat-bands of Ca located at $(\frac{1}{2}, \frac{1}{2}, 0)$ are plotted in Fig. 3. Ca d_{xy} and d_{z^2} have orbital density pointing towards four nearest Bi ions and two nearest P ions respectively, so their orbital energies are close and higher than the rest. On the other hand, $d_{x^2-y^2}$ orbital lies lowest in energy as its orbital density does not point towards any negative ions, and seperates the highest d band by 2.8 eV.

This value changes to 3.6 eV and 3.3 eV by replacing Ca with Sr and Ba respectively. The d_{xz} and d_{yz} orbitals of Ca on $x-y$ plane are symmetrically related so their eigenvalues are degenerate and lie between the other non-degenerate bands. The Pn_A p bands mix with the Ae d bands around the Γ point, with a substantial band gap throughout the rest of the zone. Notice that the conduction band minimum at Γ point consists of a mixture of various s characters, where about half of it contributed equally from the three Ca 4s, a quarter of it come from the Bi 6s and one-tenth of it supplied by the P 3s. This extended S-like state is important to the band inversion (see section III C).

Pressure increases band widths by increasing the interatomic hopping amplitudes. A band gap will decrease with a smaller volume, ultimately leading to a zero gap and band inversion. If the gap is zero or negative, the effects arising from relative energy shifts and increased mixing will be more involved. Since the heavier anion provides the states at the valence band maximum and larger pnictides have larger SOC strength, if the band gaps are small, zero, or negative, this antiperovskite structure is favorable for producing TI phases. However, because the inverted bands at Γ have double degeneracy other than the spin degeneracy, the parity is still even[18].

Focusing on the energy band gap ε_g of those stable compounds (bottom left diagonal of Table I), most of them show a small positive band gap, which is a good sign for topological insulator as the bands could be easily inverted by SOC, while some exhibit a small negative indirect band gap, which could be easily opened up by strain.

C. Topological analysis

The Z_2 invariant ν_0 determines the topological nature of an insulator, and for inversion symmetric crystals, the parity criteria proposed by Fu and Kane[14] determine the topological character. Specifically, the sum of the parities δ_i at occupied states at the TRIMs determine one of the Z_2 invariants ν_0:

$$(-1)^{\nu_0} = \prod_{i=1}^{8} \delta_i \tag{2}$$

As shown in Table I, the electronic structure (Fig. 4) and topological nature of these compounds can be classified into three categories: I) a small gap with a topologically trivial phase (e.g. Ca_3BiN in Fig. 4a), II) valence band maximum (VBM) and conduction band minimum (CBM) touching at Γ point with a Z_2 index of 1;000 (e.g. Ca_3BiP in Fig. 4b), III) possesses electron and hole pockets along high symmetry lines with Z_2 index of 1;000 (e.g. Sr_3BiP in Fig. 4c). For the first type, the band inversion does not occur with SOC turned on, but the addition of proper strain could invert the band ordering to produce a topological insulator. Sun et al.[1] claimed that

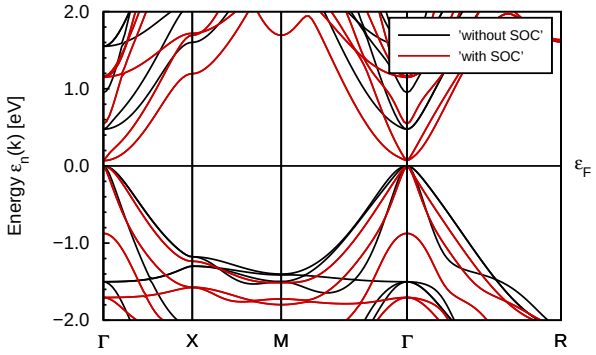

(a) Ca_3BiN - normal insulator with small gap.

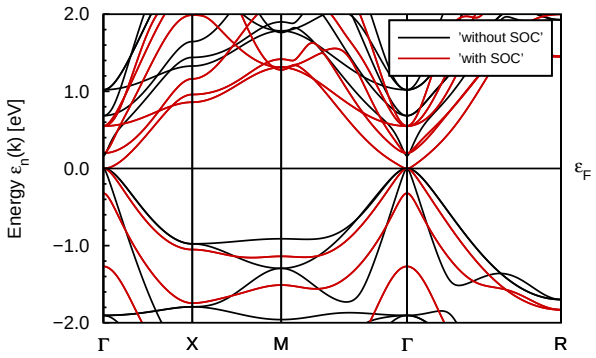

(b) Ca_3BiP - topological semimetal with CBM and VBM touching.

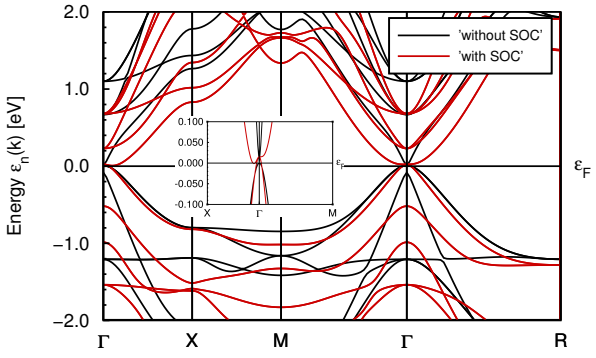

(c) Sr_3BiP - topological semimetal with hole pockets.

FIG. 4: The *Ae-Pn* antiperovskite compounds can be classified into three categories based on their electronic structure and topological invariants. Electronic band structure of Ca_3BiN, Ca_3BiP and Sr_3BiN are used as an example for each category.

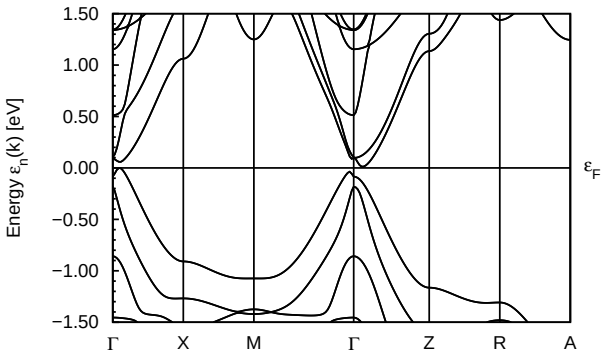

FIG. 5: Even though 7% tetragonal stretching distortion in the *ab* plane inverts the band ordering of Ca_3BiN, there is no bulk band gap as shown in the band structure.

TABLE II: Product of parity eigenvalues of the six occupied states at TRIMs indicates a 1;000 STI.

TRIM	Γ (000)	X (100) ×2	Z (001)	M (110)	R (011) ×2	A (111)
δ	-	-	-	+	+	-

Ca_3BiN can be a topological insulator with 7% tetragonal stretching distortion in the *ab* plane, however, our calculation suggests otherwise. The band structure similar to the Fig. 3(c) in reference[1] is plotted in Fig. 5 with a complete high-symmetry k-points. It is obvious that the CBM along Γ - Z and the VBM along Γ - X happen to be at the same energy level, so there is no bulk band gap. For the second and third types (highlighted in bold in Table I), the band inversion is induced by the SOC, as heavy elements like bismuth supply strong SOC effect[19], however, it does not open up a gap, leaving the system to be in a topological semimetallic phase. Since lowering the crystal symmetry lifts degeneracies, shifts bands and therefore can open up gaps, it is possible to use strain to induce a transition from topological semimetal to topological insulator, provided that the band overlapping (especially for type III) is not greater than the effect of SOC.

A case study of Ca_3BiP is used to demonstrate the role of spin-orbit coupling and strain play in the band inversion picture for the second and third class of *Ae-Pn* antiperovskite compounds. Fig. 6 shows the schematic energy level diagram of Ca_3BiP at the Γ point. For cubic Ca_3BiP, the valence states seperate the conduction states by a small energy gap of 0.2 eV. At the Γ point, the valence bands comprised of Bi 6p characters and P 3p characters have negative parities, while the extended S (ext S)-like character at the conduction band minimum has a positive parity. Since Bi has a strong spin-orbit coupling effect, the band ordering is inverted by pushing the extended S character below the top of the Bi p valence band. This band inversion mediated by strong SOC effect of Bi is also observed in the cubic perovskite $YBiO_3$[19]. However, in the case of cubic antiperovskite Ca_3BiP, it does not open the band gap, resulting in a topological semimetal phase. With a tetragonal compression of 5% along (001) in addition to the SOC, the degeneracy is lifted and a small band gap of 34 meV is produced while maintaining the inverted band ordering as shown in Table II. The strain does not violate the inversion symmetry, but merely split the degeneracy of the Γ_8^- band at the Fermi level into two sets of Kramer doublets, with odd parity below the Fermi level and even parity above the Fermi level, so the parity eigenvalues are unchanged. This mechanism is similar to that of $\alpha - Sn$ and HgTe topological insulators[10,14].

The transition from the topological semimetal state to a topological insulator can also be realized by compressing the lattice parameter c by about $1 - 7\%$, which is equivalent in symmetry to expanding both lattice parameters a and b. As shown in Fig. 7, a small energy band gap with SOC is produced within this range, with a maximum gap of only 40 meV occuring at 3% compression. The band parity remain odd within this range, but goes back to even at 8% compression. On the other hand, uniaxial expansion along the c-axis opens up a gap except along k_z, where a Dirac-like bands crossing occurs, producing a topological Dirac semimetal (Fig. 6 (f)). This will be addressed in detail in section III E. However, not all direction of strain application will open up a gap. For example, applying unaxial strain along (111) direction does not open up a gap, because the Bi p_x, p_y and p_z characters still remain equivalent.

The role of each element in the antiperovskite compounds is studied, using Ca_3BiP as an example, by examining the eigenvalues at Γ point (Fig. 8). Switching the Pn_A elements does not change the relative position of the eigenvalues of valence p bands and conduction d bands, however, the extended S (ext S)-like character, which plays a crucial role in the band inversion, varies within 0.5 eV above the Fermi level. The closer the extended S band near the Fermi level or the larger the Pn_A element, the smaller the strain and SOC required to invert the band ordering. Using the examples in Fig. 8a, Ca_3BiP needs only SOC to invert the band ordering and as small as 1% of uniaxial compression to produce a topological insulator, while Ca_3AsP requires at least 8% of strain to turn into a topological insulator.

Even though the Pn_B p bands lie at the lowest valence state, its influencial on the eigenvalue of extended S band is indelible. As shown in Fig. 8b, the eigenvalue of the extended S band decreases monotonically with increase in size of the Pn_B element. With element heavier than P in group 15, the band inversion has occured without SOC. Expanding the size of the *Ae* elements also brings down the extended S character and narrows the gap between the top and bottom valence bands (Fig. 8c).

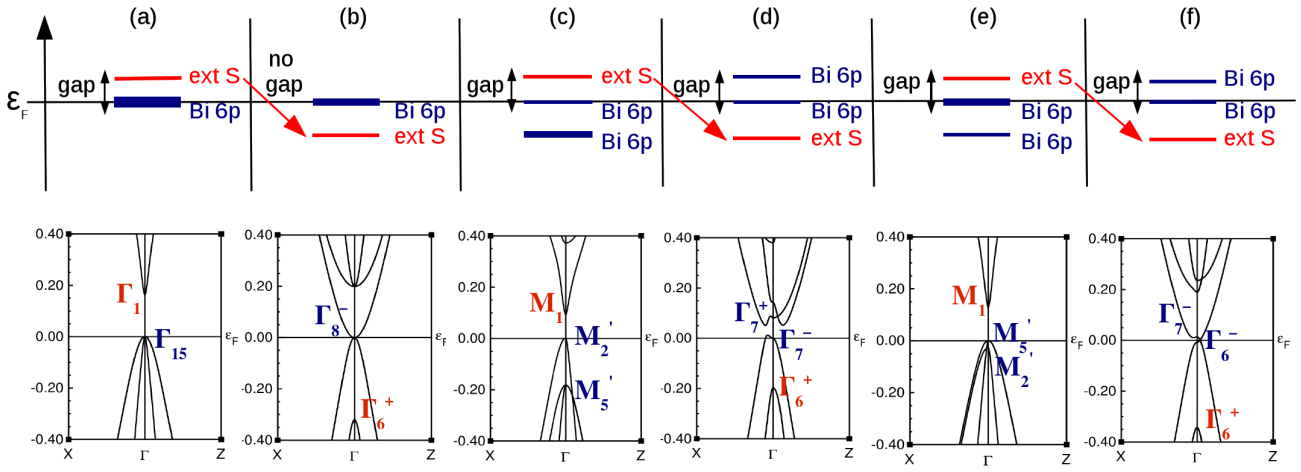

FIG. 6: Upper panel: Schematic energy diagram of Ca_3BiP at Γ point (a) without SOC, (b) with SOC, (c) with compressive strain and without SOC, (d) with 5% compressive strain and SOC, (e) with 1% expansive strain and without SOC and (f) with expansive strain and SOC. Ultra-fine, fine and thick lines represent 1-fold, 2-fold and 3-fold degeneracy (not including spin degeneracy) respectively. Ext S represents extended S-like state (see text). Lower panel: Band structures along X – Γ – Z with irreducible representations given (in Bouckaert-Smoluchowski-Wigner notation) at the Γ point.

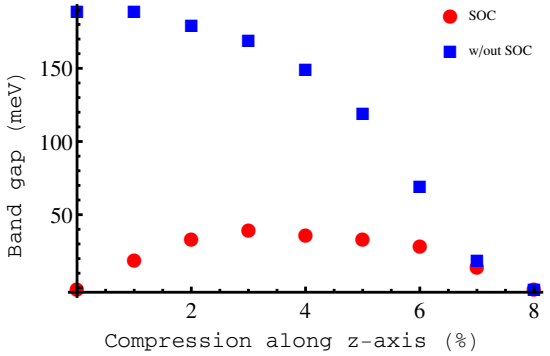

FIG. 7: Compression of Ca_3BiP along (001) without SOC closes the band gap. When SOC is turned on, the band gap is closed, but is opened up by strain.

D. Topological surface states

The existence of topological surface states is an important property of a topological insulator. Not only does it serve as strong evidence of the topologically non-trivial phase, it also serves directly as a bridge to experiments. They are known to be robust under disorder, expect when introduced with magnetic impurities where the time-reversal symmetry will be broken[20]. To calculate the surface states of (001)-strained Ca_3BiP, we first obtained the maximally-localized Wannier functions hopping parameters using ab-initio method[21,22]. We then construct a semi-infinite system and the surface spectrums are calculated using the iterative surface Green's function method[23,24] with a tight binding hopping cut-off of 4 unit cells. As shown in Fig. 9, the topological surface states terminated on (001) and (100) surfaces have gap-

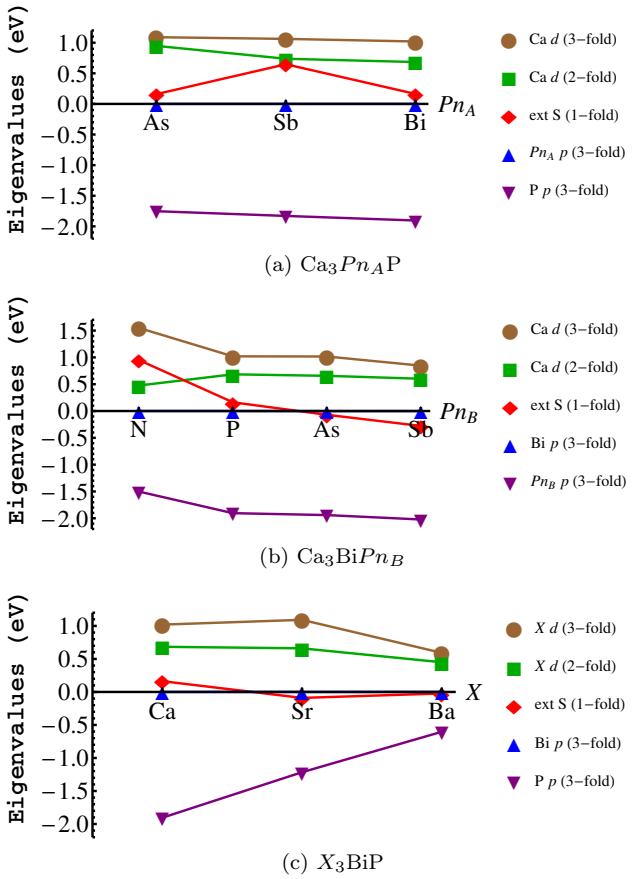

FIG. 8: Eigenvalues around the Fermi level at Γ point with different elemental substitution in Ca_3BiP (without SOC). The degeneracies are constrained by the cubic symmetry.

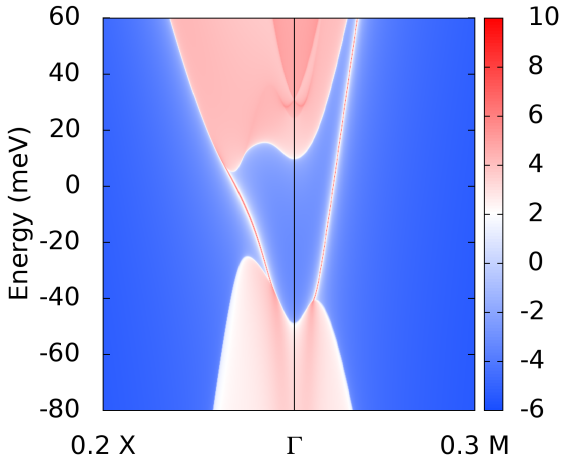

(a) (001) surface.

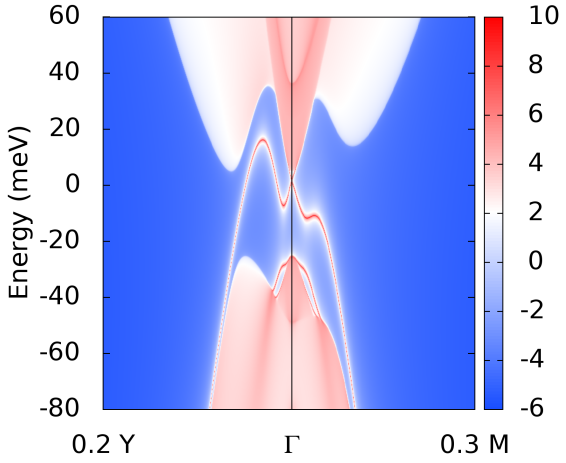

(b) (100) surface.

FIG. 9: Energy and momentum dependent spectral density of a semi-infinite crystal of (001)-compressed Ca_3BiP terminated on (001) and (100) surfaces. Warmer colors represent higher intensity. All have surface bands crossing the bulk band gap.

less surface states within the bulk band gap. Both surface projections have about the same energy bulk band gap, which is about 30 meV. The surface on (001) has topological surface bands connect the valence and conduction states, while the topological surface bands crossing the bulk band gap on (100) surface enclose a single Dirac point. These topological surface states are similar to those observed in Bi_2Te_3, Sb_2Te_3 and Bi_2Se_3[6].

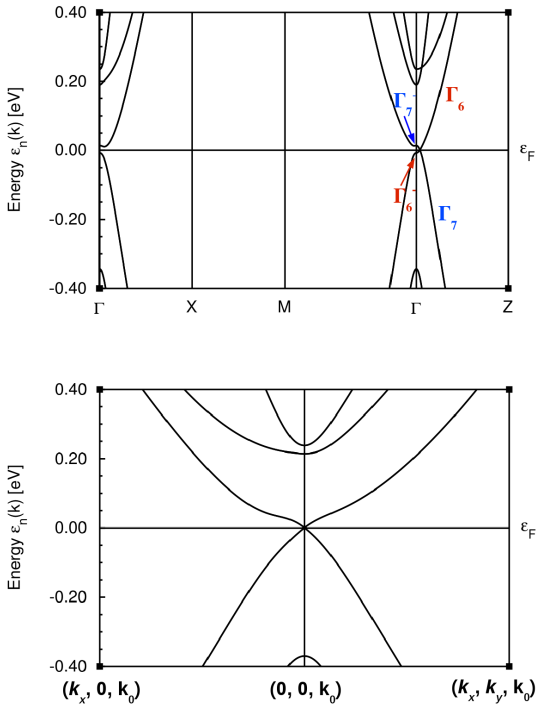

FIG. 10: Upper panel: Band structure of Ca_3BiP with tetragonal expansion of 1% along (001) shows a Dirac point along k_z. Lower panel: Band dispersion in the plane passing through the Dirac point (0,0,k_0), where $k_0 = 0.023$ Å^{-1}. Both with SOC.

E. Topological Dirac semimetal

Expansion of lattice parameter c of Ca_3BiP by 1 - 5% also lowers the crystal symmetry while maintaining the band inversion, but it does not produce a topological insulator. The calculated band structure of (001)-expanded Ca_3BiP as shown in Fig. 10 displays a gapped band structure except a band crossing with linear dispersion and 4-fold point degeneracy (including spins) along $\Gamma - Z$. This accidental band crossing is a signature of a quadrupole Dirac points, and is unavoidable as the bands have different irreducible representations, i.e. Γ_6 and Γ_7, as characterized and protected by the C_{4v} rotational point group symmetry.

Probing the surface state on (100) surface shows topological surface bands crossing the projected bulk band gap of about 20 meV (Fig. 11). The Fermi surface exhibits two non-trivial Fermi arcs touching at the Dirac points (0,0,$\pm k_0$) protected by both inversion and time-reversal symmetries. This single pair of Fermi arcs connecting two Dirac points, like the Fermi arc connecting Weyl points in a Weyl semimetal, is possible to exist as a Dirac point can be treated as two Weyl points with opposite chirality, which in this case do not annilate each other since the degeneracy is protected by the crystal

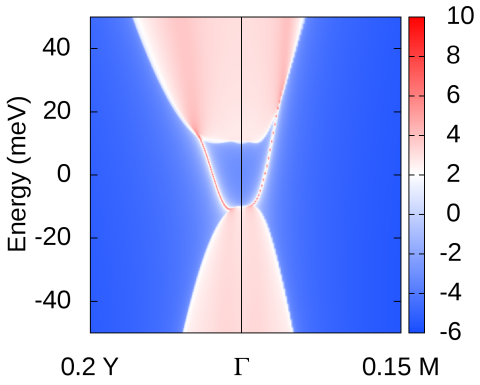

(a) Surface state on (100) surface.

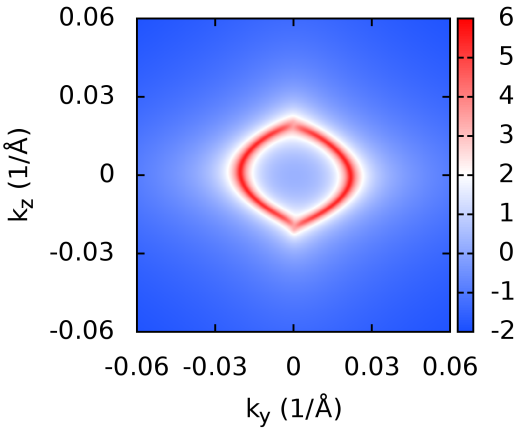

(b) Fermi arc on (100) surface.

FIG. 11: (a) Energy and momentum dependent spectral density of a semi-infinite crystal of (001)-expanded Ca_3BiP terminated on (100) surface. (b) The corresponding Fermi surface shows two half-circle Fermi arcs connecting two Dirac points along k_z.

symmetry.

This Dirac semimetal, like the rest, are protected by the time-reversal and inversion symmetries. Breaking one of these may create a single pair of Weyl points and result in a Weyl semimetal. However, breaking one of these symmetries is not an easy task. Firstly, the (anti-)perovskite structure has high symmtery so breaking the inversion symmetry can be difficult. Secondly, none of the alkaline earth and pnictide elements are magnetic. Applying magnetic field may break the time-reversal symmtery but could be difficult as the compounds are not susceptible to magnetism. Roughly estimate, 1 meV change in energy requires at least 17 T of magnetic field.

IV. SUMMARY

Spin-orbit coupling and strain are important to the topological nature of alkaline earth-pnictide antiperovskite compounds. The electronic stuructures of these compounds with SOC can be classified into three categories. First, one common class of the topological aspect is that the electronic structure is gapped with a topologically trivial phase. Second, a zero gap semiconductor with VBM and CBM touching at Γ point with a Z_2 invariant of 1;000. Third, a semimetal consists of electron or hole pockets of maximum 0.1 eV energy and band degenerate at Γ point with a Z_2 index of 1;000. Strain is required to produce a topological insulator. While the first type (e.g. Ca_3BiN[1]) needs both SOC and proper strain to have band ordering inverted, the second and third types (e.g. Ca_3BiP and Sr_3BiP) only need SOC to induce the band inversion, giving a Z_2 invariant of 1;000, but in a topological semimetal state, whereupon compressive strain may produce a transition to topological insulator. On the other hand, expansive strain may give rise to Dirac semimetals, where the single pair of Dirac points is protected by the C_{4v} rotational symmetry. With proper strain engineering, some may become a promising topological insulator and Dirac semimetal, as witness in our calculation on Ca_3BiP and Sr_3AsP antiperovskite compounds.

[1] Y. Sun, X.Q. Chen, S. Yunoki, D. Li and Y. Li, New family of three-dimensional topological insulators with antiperovskite structure, *Phys. Rev. Lett.* **105**, 216406 (2010).

[2] M.Z. Hasan and C.L. Kane, *Colloquium* : Topological insulators. *Rev. Mod. Phys.* **82**, 3045 (2010).

[3] L. Fu, Topological crystalline insulators, *Phys. Rev. Lett.* **106**, 106802 (2011).

[4] J. Li, C. He, L. Meng, H. Xiao, C.Tang, X. Wei, J. Kim, N. Kioussis, G.M. Stocks and J. Zhong, Two-dimensional topological insulators with tunable band gaps: Single-layer HgTe and HgSe, *Scientific Reports* **5**, 14115 (2015).

[5] D. Hsieh, D. Qian, L. Wray, Y. Xia, Y.S. Hor, R.J. Cava, and M.Z. Hasan, A topological dirac insulator in a quantum spin hall phase, *Nature* **452**, 970 (2008).

[6] H. Zhang, C.X. Liu, X.L. Qi, X. Dai, Z. Fang, and S.C. Zhang, Topological insulators in Bi_2Se_3, Bi_2Te_3 and Sb_2Te_3 with a single dirac cone on the surface, *Nat. Phys.* **5**, 438 (2009).

[7] W. Zhang, R. Yu, H.J. Zhang, X. Dai, and Z. Fang, First-principles studies of the three-dimensional strong topological insulators Bi_2Te_3, Bi_2Se_3 and Sb_2Te_3, *New Journal of Physics* **12**, 065013 (2010).

[8] O.V. Yazyev, J.E. Moore, and S.G. Louie, Spin polarization and transport of surface states in the topological insulators Bi_2Se_3 and Bi_2Te_3 from first principles, *Phys. Rev. Lett.* **105**, 266806 (2010).

[9] R. Li, Q. Xie, X. Cheng, D. Li, Y. Li, and X.Q. Chen, First-principles study of the large-gap three-dimensional topological insulators M_3Bi_2 (M = Ca, Sr, Ba), *Phys. Rev. B* **92**, 205130 (2015).

[10] Y. Ando, Topological insulator materials, *J. Phys. Soc. Jpn.* **82**, 102001 (2013).

[11] T.H. Hsieh, J. Liu, and L. Fu, Topological crystalline insulators and dirac octets in antiperovskites, *Phys. Rev. B* **90**, 081112 (2014).

[12] R.Yu, H. Weng, Z. Fang, X. Dai, and X. Hu, Topological node-line semimetal and dirac semimetal state in antiperovskite Cu_3PdN, *Phys. Rev. Lett.* **115**, 036807 (2015).

[13] H. Jin, J. Im, and A.J. Freeman, Topological insulator phase in halide perovskite structures, *Phys. Rev. B* **86**, 121102 (2012).

[14] L. Fu and C.L. Kane, Topological insulators with inversion symmetry, *Phys. Rev. B* **76**, 045302 (2007).

[15] R. Niewa, Alkaline-earth metal nitrides of the main-group elements: Crystal structures and properties of inverse perovskites, *Zeitschrift fr anorganische und allgemeine Chemie* **639**, 1699 (2013).

[16] J.P. Perdew, K. Burke, and M. Ernzerhof, Generalized gradient approximation made simple, *Phys. Rev. Lett.* **77**, 3865 (1996).

[17] K. Koepernik and H. Eschrig, Full-potential nonorthogonal local-orbital minimum-basis band-structure scheme, *Phys. Rev. B* **59**, 1743 (1999).

[18] T. Kariyado and M. Ogata, Low-energy effective hamiltonian and the surface states of Ca_3PbO, *J. Phys. Soc. Jpn.* **81**, 064701 (2012).

[19] H. Jin, S.H. Rhim, J. Im, and A.J. Freeman, Topological oxide insulator in cubic perovskite structure, *Scientific Reports* **3**, 1651 (2013).

[20] Y.L. Chen, J.H. Chu, J.G. Analytis, Z.K. Liu, K. Igarashi, H.H. Kuo, X.L. Qi, S.K. Mo, R.G. Moore, D.H. Lu, M. Hashimoto, T. Sasagawa, S.C. Zhang, I.R. Fisher, Z. Hussain and Z.X. Shen, Massive dirac fermion on the surface of a magnetically doped topological insulator, *Science* **329**, 659 (2010).

[21] N. Marzari, A.A. Mostofi, J.R. Yates, I. Souza, and D. Vanderbilt, Maximally localized wannier functions: Theory and applications, *Rev. Mod. Phys.* **84**, 1419 (2012).

[22] P. Blaha, K. Schwarz, G.K.H. Madsen, D. Kvasnicka, and J. Luitz, *WIEN2K, An Augmented Plane Wave + Local Orbitals Program for Calculating Crystal Properties*, Karlheinz Schwarz, Techn. Universität Wien, Austria, 2001.

[23] M.P. Lopez Sancho, J.M. Lopez Sancho, J.M.L. Sancho, and J. Rubio, Highly convergent schemes for the calculation of bulk and surface green functions, *Journal of Physics F: Metal Physics* **15**, 851 (1985).

[24] Q. Wu and S. Zhang, Github (2016).